Geochemistry, Geophysics, Geosystems

RESEARCH ARTICLE
10.1029/2020GC009558

Key Points:

- The study measures local splitting recorded by Southern Alaska Lithosphere and Mantle Observation Network network (ZE) stations
- There is a sharp transition from trench-perpendicular splitting pattern in the backarc to trench-parallel in the forearc
- Variations in splitting requires distinct anisotropy regimes below the arc, forearc, and subducting plate

Supporting Information:

Supporting Information may be found in the online version of this article.

Correspondence to:

C. Richards,
csrichards2@alaska.edu

Citation:

Richards, C., Tape, C., Abers, G. A., & Ross, Z. E. (2021). Anisotropy variations in the Alaska subduction zone based on shear-wave splitting from intraslab earthquakes. *Geochemistry, Geophysics, Geosystems*, *22*, e2020GC009558. https://doi.org/10.1029/2020GC009558

Received 1 DEC 2020
Accepted 2 MAY 2021

Anisotropy Variations in the Alaska Subduction Zone Based on Shear-Wave Splitting From Intraslab Earthquakes

Cole Richards[1], Carl Tape[1], Geoffrey A. Abers[2], and Zachary E. Ross[3]

[1]Geophysical Institute, University of Alaska Fairbanks, Fairbanks, AK, USA, [2]Department of Earth and Atmospheric Sciences, Cornell University, Ithaca, NY, USA, [3]Seismological Laboratory, California Institute of Technology, Pasadena, CA, USA

Abstract Shear-wave splitting observations can provide insight into mantle flow, due to the link between the deformation of mantle rocks and their direction-dependent seismic wave velocities. We identify anisotropy in the Cook Inlet segment of the Alaska subduction zone by analyzing splitting parameters of S waves from local intraslab earthquakes between 50 and 200 km depths, recorded from 2015–2017 and emphasizing stations from the Southern Alaska Lithosphere and Mantle Observation Network experiment. We classify 678 high-quality local shear-wave splitting observations into four regions, from northwest to southeast: (L1b) splitting measurements parallel to Pacific plate motion, (L1a) arc-perpendicular splitting pattern, (L2) sharp transition to arc-parallel splitting, and (L3) splitting parallel to Pacific plate motion. Forward modeling of splitting from various mantle fabrics shows that no one simple model fully explains the observed splitting patterns. An A-type olivine fabric with fast direction dipping 45° to the northwest (300°)—aligned with the dipping slab—predicts fast directions that fit L1a observations well, but not L2. The inability of the forward model fabrics to fit all the observed splitting patterns suggests that the anisotropy variations are not due to variable ray angles, but require distinct differences in the anisotropy regime below the arc, forearc, and subducting plate.

Plain Language Summary Mantle flow can cause seismic wave velocity to become directionally dependent (seismic anisotropy) and is related to the flow direction. Using a dense temporary seismic transect along the Cook Inlet segment of the Alaska subduction zone, we identify four distinct regions of anisotropy. This includes a sharp transition from arc-parallel fast directions in the forearc to arc-perpendicular fast directions in the backarc. Forward modeling of various mantle fabrics shows that no one simple model fully explains the anisotropy and requires distinct differences in the anisotropy regimes below the arc, forearc, and subducting plate.

1. Introduction

The Cook Inlet region of south-central Alaska is located toward the eastern end of the 4,000 km-long Aleutian–Alaska subduction zone, where the Pacific plate subducts under North America. Plutonic rocks and basin-deposited strata indicate that subduction has persisted in this region for more than 200 Ma (Fisher & Magoon, 1978; Jarrard, 1986). The Cook Inlet segment of the subduction zone exhibits abundant seismicity down to approximately 200 km depth, as well as active volcanoes (Figure 1). Here, we use recordings from these intraslab earthquakes to characterize the anisotropic structure of the subduction zone.

Plate motion has often been linked to shearing and flow in the upper mantle (Long & Wirth, 2013), including viscous coupling between the downgoing slab and the overlying mantle (van Keken, 2003). Shear-wave splitting has been utilized to study anisotropy in both the crust and upper mantle in various regions around the globe (Savage, 1999; Silver & Chan, 1991). In subduction zones, it is predicted that multiple types and layers of olivine fabrics and other sources of anisotropy may be present (Jung & Karato, 2001; Karato et al., 2008; Silver & Savage, 1994). Changes in olivine fabric have been evoked to explain sharp transitions of shear-wave splitting fast directions from arc-parallel in the arc and forearc to arc-perpendicular in the backarc without requiring a change in mantle flow direction (Nakajima & Hasegawa, 2004; Kneller et al., 2005). However, even a small presence of other mantle minerals, such as antigorite, can have a strong influence on the observed splitting pattern (Horn et al., 2020). Furthermore, organized melt channels can be

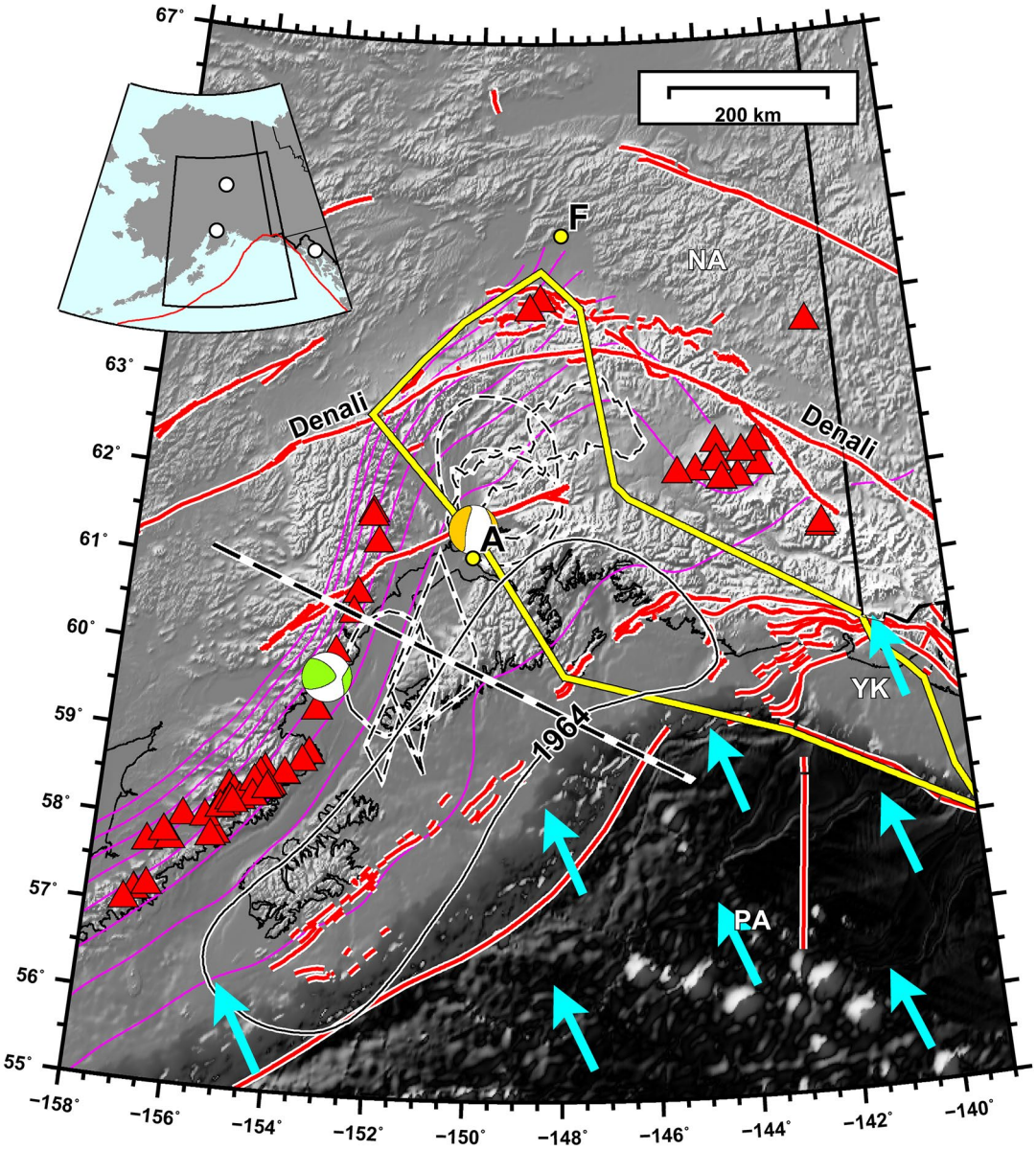

Figure 1. Active tectonic setting of the Aleutian-Alaskan subduction zone, south-central Alaska. Cyan arrows show the plate vectors for the subducting Pacific plate (PA) relative to fixed North America (NA) (Argus et al., 2011). Red lines denote active faults (Koehler et al., 2012). Magenta curves are the 20 –160 km contours of the subduction interface, that is, the top of the Pacific plate (Hayes et al., 2018). Yellow bounded region denotes the surface and subsurface extent of the Yakutat block (YK) (Eberhart-Phillips et al., 2006). Red triangles represent active volcanoes. Black dashed lines are inferred slow slip and tremor events from various sources (Fu & Freymueller, 2013; Li et al., 2016; Ohta et al., 2006; Wech, 2016; Wei et al., 2012). Green and white beachball is the seismic moment tensor of the January 24, 2016 M_w 7.1 Iniskin earthquake. Orange and white beachball is the seismic moment tensor of the November 30, 2018 M_w 7.1 Anchorage earthquake. Also marked is the aftershock zone of the 1964 M_w 9.2 earthquake (Davies et al., 1981). Black and white dashed line, through Redoubt volcano, denotes the profile for all cross sections shown in this study. A = Anchorage, F = Fairbanks.

a source of anisotropy (Holtzman & Kendall, 2010). Although there are exceptions (Hammond et al., 2010; Schlaphorst et al., 2017), most local splitting studies around the globe have suggested that the mantle wedge is the main anisotropic structure in the subduction system (Abt et al., 2009; León Soto & Valenzuela, 2013; Long & van der Hilst, 2006; Nakajima & Hasegawa, 2004). In the Alaska subduction zone specifically, anisotropy has been suggested to be present in the mantle wedge and in the subducting Pacific lithosphere and subslab asthenosphere (Christensen & Abers, 2010; Hanna & Long, 2012; Karlowska et al., 2021; McPherson et al., 2020; Perttu et al., 2014; Song & Kawakatsu, 2013; Venereau et al., 2019).

Globally, the two most common splitting patterns for local splitting studies are arc-parallel and a transition from arc-parallel in the forearc to arc-perpendicular in the backarc (Long & Wirth, 2013). There have been few local splitting studies in Alaska, they all lack dense station coverage in the backarc, and they show a range of different splitting patterns for various sections of the subduction zone. Karlowska et al. (2021) used 23 Transportable Array (TA) stations and observed arc-parallel fast directions in the forearc transitioning to arc perpendicular in the backarc. Wiemer et al. (1999) used three stations and showed arc-parallel fast directions in the forearc, along with several arc-perpendicular measurements in the backarc near Redoubt volcano. Christensen et al. (2003) published preliminary results that show roughly the opposite transition (arc-perpendicular in the forearc to arc-parallel) occurring further northeast where the slab dip is shallow; these results were included in the compilation by Long and Wirth (2013). Hacker and Abers (2012) showed only a single example. Yang et al. (1995) showed a mostly arc-parallel pattern in the Shumagin Islands.

There have been numerous SKS splitting studies in Alaska and its subduction zone over the past decade (Christensen & Abers, 2010; Hanna & Long, 2012; McPherson et al., 2020; Perttu et al., 2014; Venereau et al., 2019). These studies benefitted from temporary enhanced station coverage in the easternmost subduction segment, where a gap in volcanism is associated with subduction of the thick Yakutat terrane (Figure 1) (Eberhart-Phillips et al., 2006; Ferris et al., 2003; Rondenay et al., 2010). In this eastern segment, the SKS splitting pattern abruptly transitions from arc-perpendicular southeast of the 70 km depth contour of the subduction interface to arc-parallel northwest of the 70 km contour (Christensen & Abers, 2010). The arc-parallel pattern is usually attributed to along-arc flow in the mantle wedge, while the arc-perpendicular pattern is attributed to a combination of entrained asthenospheric flow in the plate convergence direction beneath the subducting Pacific plate, as well as fossil anisotropy within the subducting plate (Christensen & Abers, 2010; Hanna & Long, 2012; McPherson et al., 2020; Perttu et al., 2014; Venereau et al., 2019).

Here, we focus on a recent deployment of seismic stations in the Cook Inlet region to establish a large data set of shear-wave splitting measurements from local intraslab earthquakes. We identify three regions of splitting measurements: Region L1a in the backarc region, revealing arc-normal splitting arising from corner flow in the wedge; Region L2 overlying the cold part of the mantle wedge, revealing a NE-SW splitting direction oblique to the arc; Region L3 in the forearc region, revealing arc-normal splitting arising from anisotropy in subducted oceanic lithosphere (and possibly the crust). These local S splitting results provide a valuable complement to previous studies of SKS shear-wave splitting in Alaska. To investigate possible anisotropic structures that could explain our observations, we perform preliminary forward modeling to provide predicted splitting directions. A more extensive modeling effort is needed to systematically allow for a wide range of possible subsurface anisotropic models, while also considering all 678 local S and 360 SKS measurements.

2. Data and Methods

We measure shear-wave splitting for S waves from local intraslab earthquakes and also for SKS waves from teleseismic earthquakes. Our study focuses on local S splitting, and the SKS analysis is included in the supplement.

We examined local intraslab earthquakes recorded between January 1, 2015 and November 30, 2017 by stations from Southern Alaska Lithosphere and Mantle Observation Network (SALMON; network ZE) (Tape et al., 2017), TA (EarthScope Transportable Array), and the permanent networks of AVO (Alaska Volcano Observatory; network AV) and AEC (Alaska Earthquake Center; network AK) (Figure 2). In total, there are 84 stations that were active for all or part of this period. The SALMON network included an arc-normal line of broadband receivers traversing the Cook Inlet segment of the Alaska subduction zone at Redoubt volcano. This combination of networks, specifically SALMON, provides enhanced station coverage of the forearc, arc, and backarc.

Our region of interest contains stations and local earthquakes and is bounded by longitudes −156° to − 148° and latitudes 59°–62°. For our time period of interest, there are 12,095 events $M_l \geq 1.5$ in the Alaska Earthquake Center catalog. Only ray paths with angles of incidence smaller than 37° (0° is vertical incidence) were considered in order to avoid contamination of particle motions (Nuttli, 1961). Incidence angles and ray paths were determined using TauP (Crotwell et al., 1999) and the standard 1D velocity model used

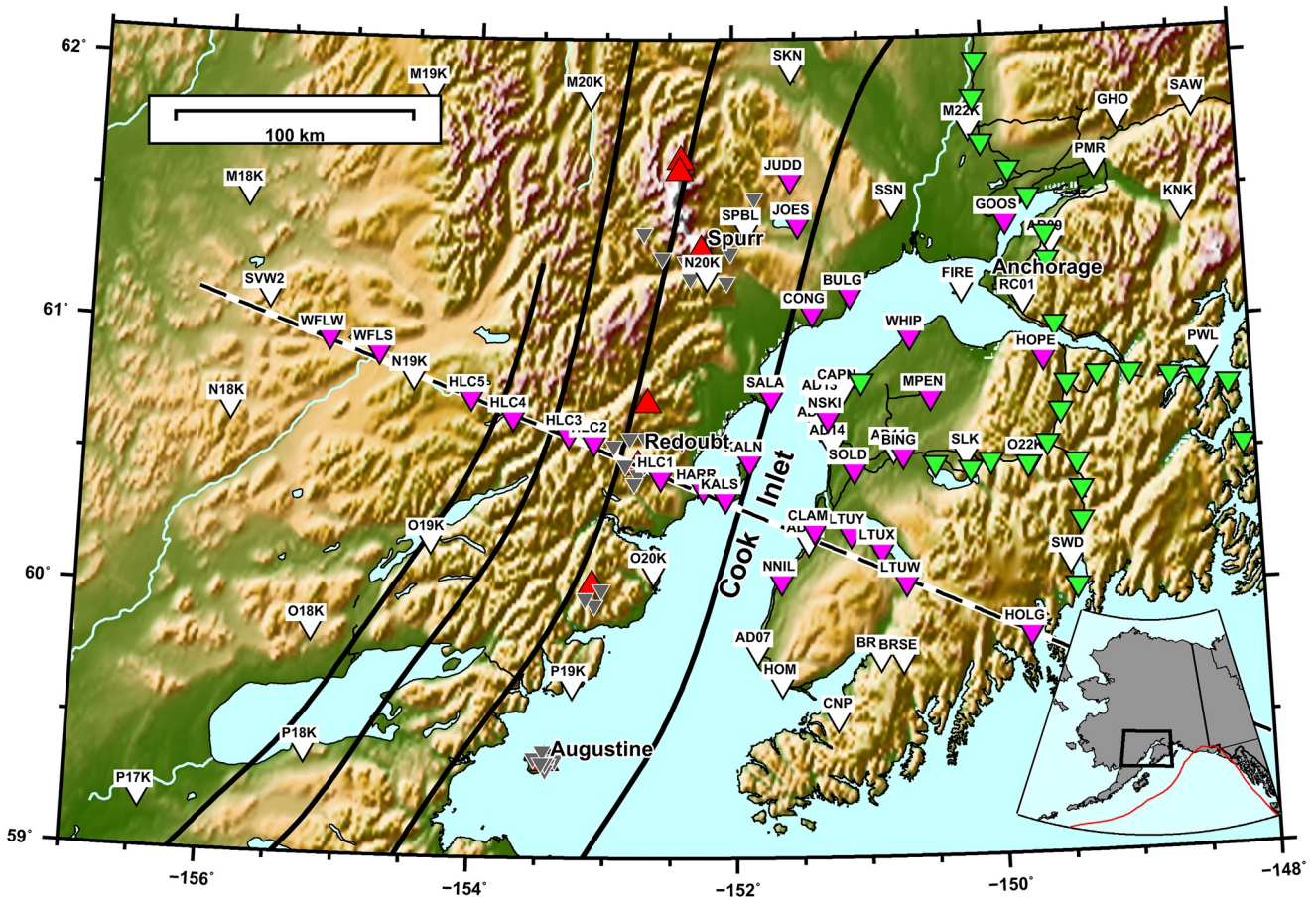

Figure 2. Seismic stations in the study region of south-central Alaska. The stations are colored by project or operator: ZE (SALMON; magenta), YE (MOOS; green), AV (AVO; gray), TA (EarthScope; white), and AK (AEC; white). Red triangles are active volcanoes, including Augustine, Redoubt, and Spurr. Black and white dashed line represents the profile through Redoubt volcano for cross-sections in other figures. Subduction contours of 50, 100, 150, and 200 km are plotted as black lines (Hayes et al., 2018).

for locating earthquakes in southern Alaska (Table S1). Automatic S phase picking (Ross et al., 2016) was performed to identify candidate S waves for measurement. Our target period range of 0.2–1 Hz for splitting measurements led to an expectedly drastic reduction of the data set, as generally only the larger events ($M_l > 3$) had sufficient signal-to-noise levels (Figure S4).

We used the software package MFAST (Savage et al., 2010; Teanby et al., 2004; Wessel, 2000), which makes splitting measurements using the eigenvalue minimization method of Silver and Chan (1991). From the Alaska earthquakes, we obtained 678 high-quality splitting measurements. Each measurement consists of a fast polarization direction ϕ and delay time δt for a given event–station pair. Each measurement is assigned a grade based on its quality. We only considered the highest-quality measurements (grade A), which have signal-to-noise ratio (SNR) > 4, error of $\delta\phi$ (one standard deviation) < 10°, $\delta t < 1.2$ s, and no other ϕ and δt pair produces a high-quality solution. Figure 3 shows an example of a grade A local splitting measurement made at backarc SALMON station HLC5. If the determined initial polarization of the shear wave is within 20° of ϕ or the orthogonal slow direction, the measurement is considered null. Null measurements indicate that the shear wave was polarized parallel to either the fast or slow axis or that no splitting occurred. We do not consider null results as there is much ambiguity in interpreting them. We also manually inspected each measurement, discarding those that showed signs of cycle skipping or non-linear particle motions.

Shear-wave splitting directions are often interpreted within the context of plate motions (Long & Becker, 2010). In our shear-wave splitting maps, we display plate velocities in five different reference frames: NNR-MORVEL (Argus et al., 2011), spreading alignment (Becker et al., 2015), a reference frame related

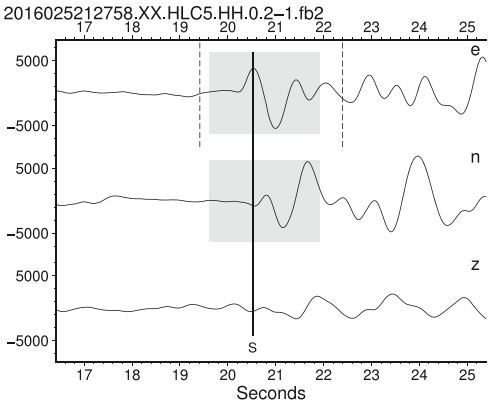

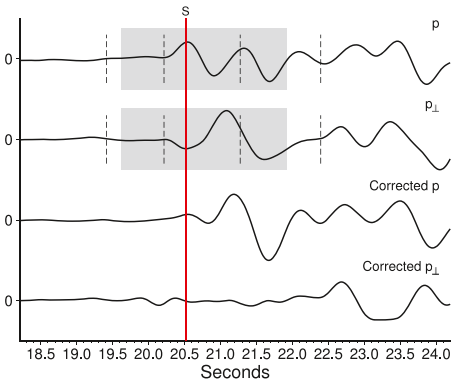

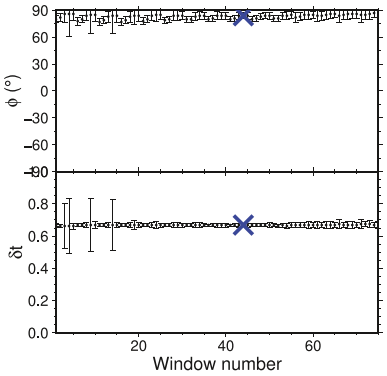

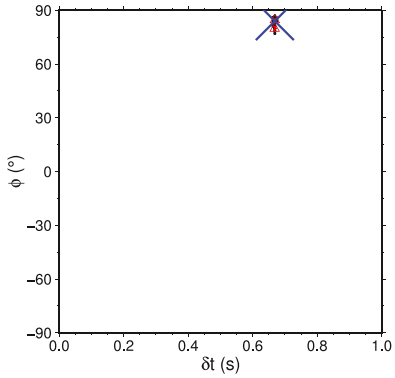

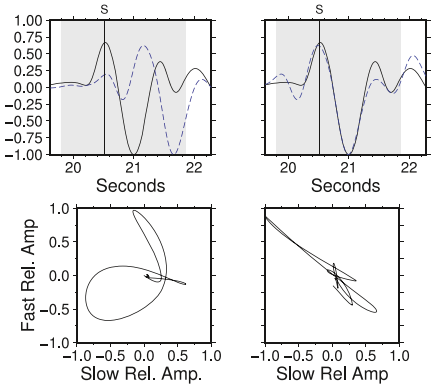

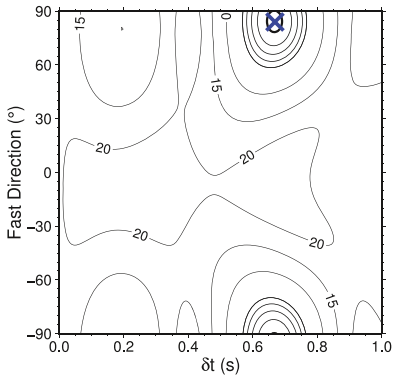

event 2016025212758.XX.HLC5.HH.

depth: 109.366 km
distance: 126.597 km
magnitude: 3.88

splitting windows (relative to S–Pick
wbeg: –1.10 – –0.30 (5)
wend: 0.76 – 1.88 (15)
selected: 19.615 – 21.915

results: GRADE ACI

fast: 84.0 +/– 3.2 (°)

δt = 0.669 +/– 0.009 (s)

spol: 130.4 +/– 0.9 (°)
fast (abc): 84.0 +/– 3.2 (°)

to global SKS splitting (SKS5) (Becker et al., 2015), a hot spot reference frame (MM07-M) (Morgan & Morgan, 2007; Doubrovine et al., 2012), and a fixed North America reference frame. While considering a fixed North America reference frame, we acknowledge that the region of south-central Alaska is not actually fixed to interior North America but in fact moves a few mm/yr to the southwest (Freymueller et al., 2008). In general, for these reference frames, at (−150°, 59°) the Pacific plate moves northwest at ∼52 mm/yr and at (−155.3°, 60.5°) the North American plate south-southwest at ∼10–20 mm/yr.

3. Results

We obtain 748 high-quality (grade A) local S shear-wave splitting measurements from earthquakes in the Cook Inlet region. These includes 678 measurements from events >50 km depth, assumed to originate within the subducting slab, and from 70 events <50 km depth, which originate in the crust or within a portion of the subducting slab that is in contact with the continental Moho. The crustal measurements are included in some figures, but our main analysis is on the measurements from deeper events.

The 678 measurements arise from earthquakes having a mean magnitude M_l 3.20 and mean depth 99 km (Figure S4). The measured splitting times are in the range of δt = 0.06–0.79 s with an average of 0.33 s. Figure S5 shows the 678 shear-wave splitting results superimposed on a map of the Cook Inlet and their rays traced through a cross section profile of the subduction zone. A subset of 357 measurements, focusing on the mantle wedge region, is shown in Figure 5.

To facilitate discussion and interpretations, we categorize the local S splitting observations into regions, defined by eye, using two approaches: (1) careful examination of patterns found in individual station maps (Richards, 2020b), and (2) examination of spatially the smoothed dataset (Richards, 2020a). The region boundaries are manually drawn in where there are abrupt transitions in the splitting fast direction. We identify four splitting regions, from west to east:

- Region L1b, plate convergence parallel pattern (north-northwest to south-southeast) for the deepest events (≥∼150 km) recorded at backarc stations (Figures 5 and 6).
- Region L1a, arc-perpendicular pattern in the arc and backarc (Figures 5 and 6).
- Region L2, mostly arc-parallel pattern in the forearc region (∼60–80 km subduction interface contour) (Figure 5, Figures S11 and S12).
- Region L3, fast directions sub-parallel to the plate convergence direction in the western portion of the Kenai Peninsula (Figure S7).

These regions can be identified even from splitting maps of single stations. For example, TA.N19K reveals the transition from L1b to L1a, while ZE.HLC4 is exclusively L1a (Figure 6). Additional stations along the transect through Redoubt volcano can be seen in Figures S09–S13

For each region, we plot rose diagrams, which count the splitting directions within azimuthal sectors. In some cases, we display two average directions: average fast direction weighted by delay time (red) and average fast direction without considering delay time (green) (e.g., Figure 5).

As is shown in Figure S5, the local shear waves densely sample the subducting slab, shallow mantle wedge, and parts of the overriding plate. Ray tracing shows that some of the measurements have sub-horizontal ray paths before steepening at shallow depths to meet the 37° incidence angle requirement (Figure 5). Therefore, most rays sample the wedge at incident angles greater than 37°. The region of the mantle wedge deeper

Figure 3. High quality (grade A) local splitting measurement, illustrated for station ZE.HLC5 for a M_l 3.9 intraslab earthquake on January 25, 2016 at 109 km depth. The figure is a standard output file from the code MFAST. The labels below are for top left (TL), middle left (ML), and so on. The gray boxes in panels (TL), (TR), and (BL) show the time window used for the final measurement. (TL) Waveforms filtered 0.2–1.0 Hz for the east (e), north (n), and vertical (z) components. The solid line is the S arrival using dbshear (Ross et al., 2016). The dashed lines are the minimum start and maximum end times for windows used in the processing, as in (TR). (TR) Waveforms rotated into the SC91-determined (Silver & Chan, 1991) incoming polarization direction (p) and its perpendicular value ($p_\perp$), for the original filtered waveform (top) and the waveforms corrected for the SC91-determined δt (bottom) for the window shown in gray. (ML) Fast direction ϕ and splitting delay time δt determined for each measurement window as a function of window number. (MR) All the clusters of five or more measurements, with the large X being the chosen cluster. (BL) Waveforms (top) and particle motion (bottom) for the original (left) and corrected (right) waveform according to the final chosen SC91 window. (BR) Contours of the smallest eigenvalue of the covariance matrix for the final chosen SC91 measurement.

than ~100 km is sparsely sampled, and no part of the wedge deeper than ~150 km is sampled, nor is the subslab mantle. In general, the forearc stations have ray paths through the slab and/or cold forearc mantle and arc/backarc stations have paths through the mantle wedge. All ray paths travel through the overriding plate.

3.1. Comparison of Local S and SKS

Our analysis of SKS data is provided in Section S1 and summarized in Figure 7. A comparison of our local S and SKS splitting results and regions is provided in Figure 8, based on the maps in Figure S5 (see also Figure 5) and Figure 7. The figures offer the following points:

1. In the furthest west backarc region (outer mantle wedge), both local S and SKS offer a mix of fast directions, including NE–SW and NW–SE.
2. In the inner mantle wedge, there is a conspicuous difference of about 45° between the E-W fast direction for local splitting (L1a) and the NE-SW fast direction for SKS splitting (L2).
3. For the cold forearc mantle wedge, ray coverage is good for local S and poor for SKS. The predominant fast splitting direction from local S is NE-SW.
4. In the forearc region of the Kenai Peninsula, both local S and SKS data reveal predominant NW-SE fast directions that are consistent with the plate convergence direction. The local S results imply that at least some of the anisotropy is between the intraslab earthquakes and the surface, that is, in the shallowest oceanic lithosphere or overlying crust.

A main challenge in comparing SKS and local S splitting is that the measurements are typically made in very different frequency ranges. Shear-wave splitting parameters are frequency dependent (Long & van der Hilst, 2006; Marson-Pidgeon & Savage, 1997; Wirth & Long, 2010), because different frequency waves for the same source–station pair are sensitive to somewhat different structures. Other difficulties arise from the different paths that the waves take. Even for overlapping S and SKS ray paths, the SKS wave has traveled the entirety of the mantle before reaching the point where the S wave originates. Allowing up to 37° incidence angles for the local S rays increases the difficulty in comparing with SKS splitting, because splitting parameters can vary depending on the angle at which the shear wave propagates through an anisotropic material. Thus, when comparing non-vertical ray paths of local events to vertical SKS paths in the same region, there may be differences in ϕ and δt. Therefore, it does not always make sense to compare directly a single station's measurements for the two phases unless the local rays are nearly vertical, the SKS rays overlap with the local rays, and the anisotropy is thought to lie between the local event and the station. Even in the ideal case of overlapping vertical ray paths, the SKS waves have much larger Fresnel zones due to their lower frequencies. For example, the first Fresnel zone for an SKS wave (dominant period 8–10 s) at 50 km depth is ~80 km wide (Favier & Chevrot, 2003; Hanna & Long, 2012). Comparatively, assuming a velocity of 4.6 km/s (Table S1) and a source at 100-km depth, the width of the first Fresnel zone at 50 km depth ranges from 8 to 19 km for periods of 0.2–1.0 s (Spetzler & Snieder, 2004). Forward modeling, as discussed in Section 4.1, it is needed to identify a range of possible models that fit the observed local S and SKS splitting measurements.

4. Discussion

The dominant pattern of the local S data set (Figure S5) is one of arc-perpendicular fast directions, characterizing region L1a. This can best be seen in Figures 5 and 6. Region L1a has splitting measurements with the majority of their ray paths in the mantle wedge. Due to the slab and station array geometry, these ray paths only exist for stations in the arc and backarc (Figure 5). Examining the relationship between δt and focal depth for stations with at least ~50 km of wedge beneath them reveals that δt slightly increases as focal depth increases (Figure 9). For measurements at these stations, an increase in focal depth typically corresponds to a longer ray path in the mantle wedge and thus a longer delay time. For example, ray paths at station N19 K show that the path through the wedge is ~110 km for focal depths near 150 km ($\delta t \approx 0.5$ s) and only ~75 km for focal depths near 85 km ($\delta t \approx 0.2$ s) (Figure S9). Splitting studies at various subduction zones around the globe, including within Alaska (Christensen & Abers, 2010; Wiemer et al., 1999), suggest an anisotropic wedge and show that δt increases with path length in the wedge.

This arc-perpendicular splitting pattern observed in region L1a is apparent in some other subduction zones, where it is often interpreted as 2D corner flow as olivine with A-type fabric is expected in the hot, dehydrated mantle wedge (Hall et al., 2000; Kneller et al., 2005; Long & Silver, 2008; Long & Wirth, 2013). Our observations support the common finding that the mantle wedge is a major contributing anisotropic structure in the subduction system, and we interpret the clear arc-perpendicular pattern in the arc and backarc to be 2D corner flow of A-type fabric.

Many of the measurements in the forearc have fast directions approximately aligned with the arc (region L2) and have ray paths that sample the cold part of the mantle wedge (Figure 5, Figures S11 and S12). Wiemer et al. (1999) and Karlowska et al. (2021) also show an arc-parallel local splitting pattern in region L2 as well as evidence of the sharp change in fast direction across the arc. The ray paths that sample the cold part of the mantle wedge all originate in the slab and have some path length in the slab. Furthermore, for this subset of measurements, the path lengths in the overriding crust are as large or larger than paths in the underlying cold mantle and in some cases the arc-parallel splitting pattern does align with geological trends. This makes it difficult to determine whether the main contributor to this splitting pattern is the underlying cold mantle, the slab, the overriding crust, or all three. Uchida et al. (2020) show a similar splitting pattern in the forearc of Japan and contribute the anisotropy to the crust.

The substantial increase in delay times from our crustal splitting measurements to these forearc measurements suggest that there is contribution from the mantle (Figure 9). This is further supported by the fact that SKS splitting patterns in this region are arc-parallel and are even less likely influenced by crustal anisotropy due to their long periods and minimal crustal sensitivity. These observations agree with the predicted 90° rotation in fast directions that occurs in 2D corner flow with B-type LPO fabric in the cold hydrated portion of the mantle wedge (Karato et al., 2008; Kneller et al., 2005). However, other explanations are possible for the change in splitting pattern observed in region L2, such as minerals other than olivine, metamorphic fabrics, aligned fluid-filled cracks, and other textures. The transition appears to take place above where the plate interface reaches the 80 km subduction interface contour.

We also observe fairly large delay times for some ray paths that sample no mantle wedge at all (Figure S6). Rays from deep events traveling to stations in the forearc sample entirely the slab and overriding crust, and yet they can have δt comparable to the measurements with similar path lengths in the mantle wedge. The long delay times provide strong evidence that the lithosphere in the subducting slab is significantly anisotropic. The measurements for paths in the slab lack any overall splitting pattern. However, a subset of the northernmost measurements, where the slab dip is more shallow, exhibits a roughly arc-parallel pattern (Figure S6). Naugler and Wageman (1973) show consistent north-south magnetic lineations related to Tertiary Farallon ridge spreading. These lineations are located immediately adjacent to the Alaska subduction zone (Maus et al., 2009) and are roughly parallel to these northern splitting fast directions (ϕ). This pattern may be due to anisotropic structure within the subducting Pacific plate related to its fossil spreading direction, but this would only explain this small subset of measurements.

The western portion of the Kenai Peninsula (region L3; Figures S5 and S7) shows fast directions sub-parallel to the plate convergence direction, has shallow focal depths (50–60 km), and exhibits short delay times ($\delta t \approx 0.2$ s). There is no mantle wedge beneath this region; these rays sample the subducting Pacific lithosphere and the overriding plate. While these measurements could be influenced by anisotropy in the overriding plate, we interpret the splitting to be in the subducting lithosphere because we have shown that the slab is substantially anisotropic. Furthermore, the delay times from crustal earthquakes (Figure 9) are shorter than those observed from paths sampling the subducting Pacific lithosphere. This interpretation of a low crustal contribution to anisotropy is supported by the results of Wiemer et al. (1999).

Our observations require a model that can explain splitting patterns of arc-perpendicular in the backarc, arc-parallel in the forearc, and plate convergence parallel in the further trenchward forearc. With the addition of an anisotropic slab, multiple subduction zone mantle flow models could explain the observed splitting patterns. The models include 2D corner flow with B-type fabric (or similar) in cold forearc part of the mantle wedge (Long & Wirth, 2013) and three-dimensional flow from along strike variations in slab dip (Kneller et al., 2007).

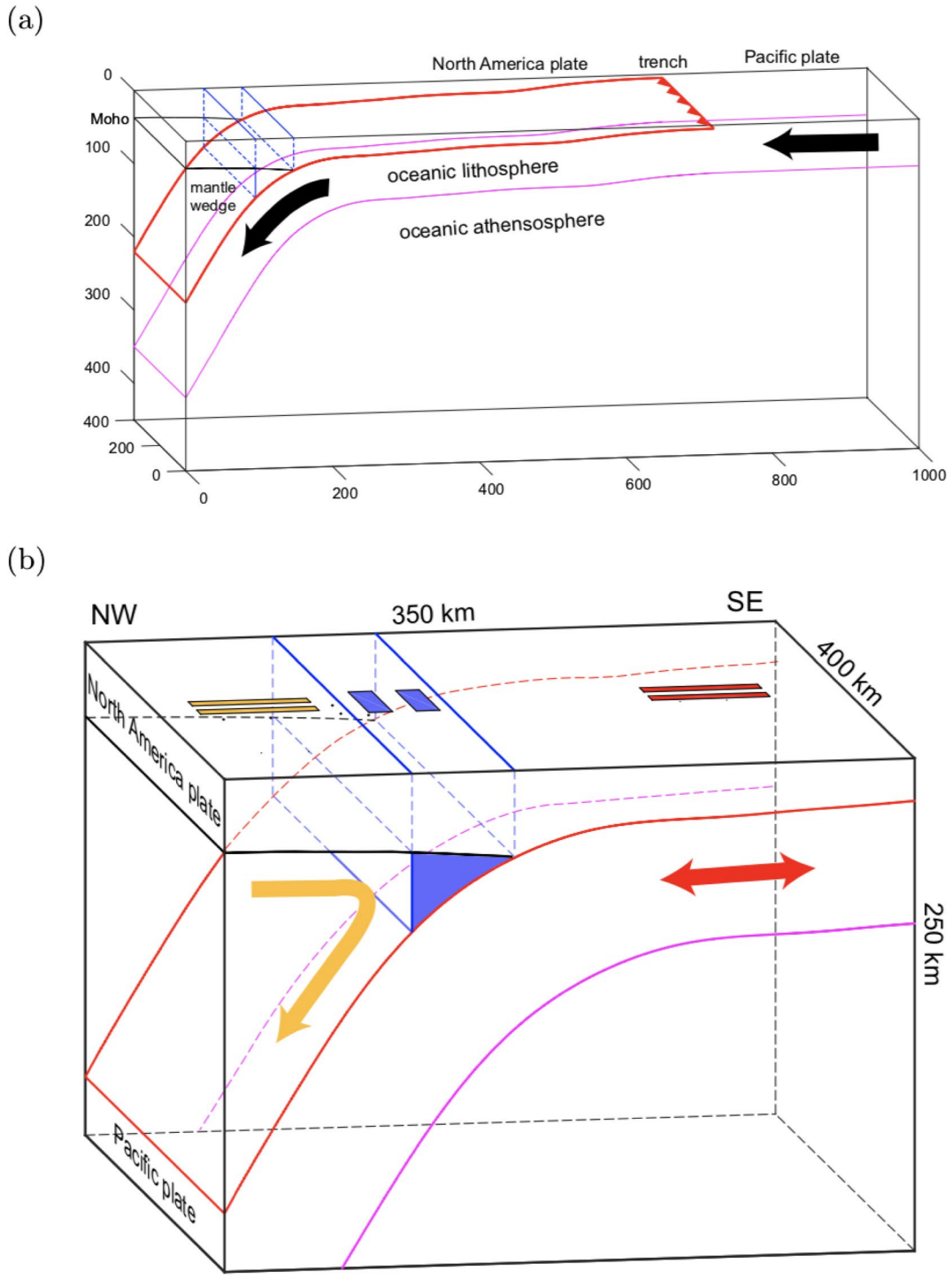

Figure 4. Cross section of the Alaska subduction zone along the profile shown in Figure 1. The slab geometry is slab2.0 (Hayes et al., 2018) (red line), and the Moho geometry is from Miller and Moresi (2018) (lower black line). (a) Full profile, including the trench. (b) Zoom-in on the upper left portion of (a). The triangular region represents the cold forearc part of the mantle wedge; its downdip extent is chosen as the point where the subduction interface is at 80 km depth. The colored arrows and symbols are described in the Discussion.

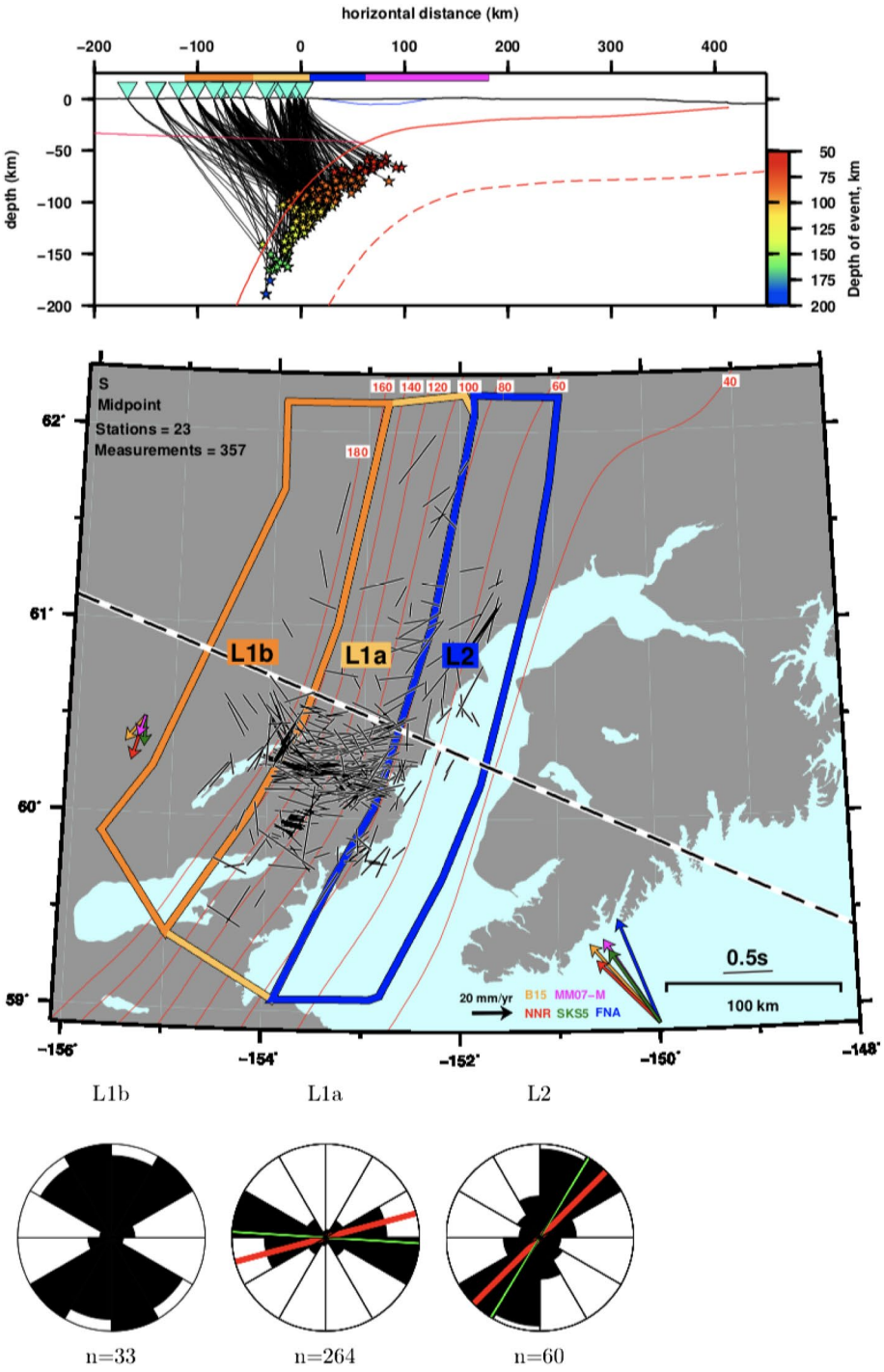

Figure 5. Local splitting measurements sampling near or within the mantle wedge. The subset of 357 measurements is for all stations having a vertical distance of ≥50 km between the continental Moho and the subduction interface. See Figure S5 for the full data set of 678 measurements, including the easternmost Region L3. Five colored arrows denote plate velocities from different plate models (see main text). (top) Ray paths (middle) Measurements plotted at the midpoint of the straight line path between hypocenter and station. The regions, from west to east, are: L1b (orange) L1a (yellow), and L2 (blue). These regions exhibit convergence-parallel fast directions in the furthest west backarc (L1b), arc-perpendicular in arc (L1a), and arc-parallel in the forearc (L2). (bottom) Rose diagrams for the splitting regions.

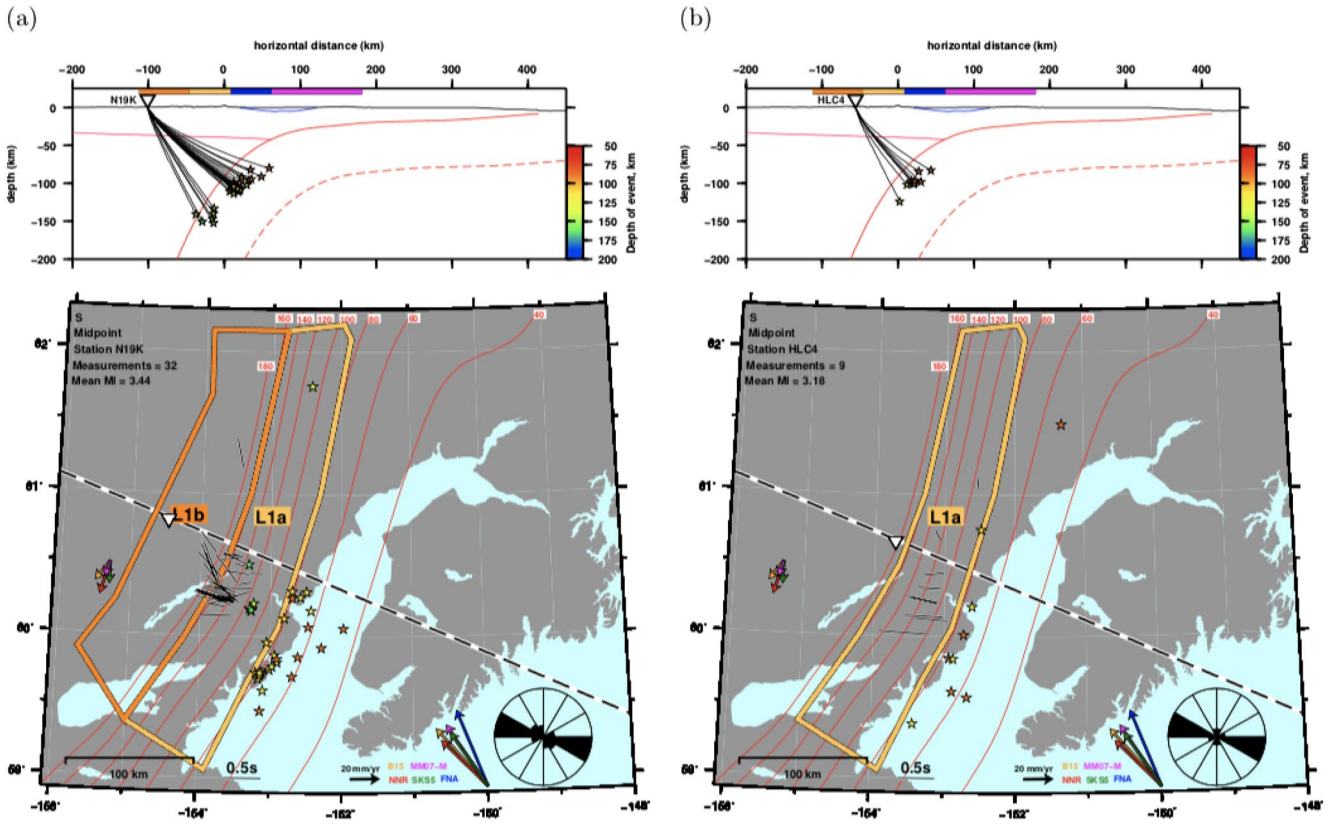

Figure 6. Local splitting measurements for stations TA.N19K (a) and ZE.HLC4 (b), both west of Redoubt volcano. TA.N19K exhibits the transition from L1a (east) to L1b (west), while ZE.HLC4 is dominantly L1a (arc normal).

Geodynamic 3D mantle flow predictions from Jadamec and Billen (2010, 2012) show flow at 100 km depth for most of our region is approximately arc-perpendicular and becomes closer to the plate convergence direction further north and further into the backarc. This agrees with the fast directions of regions L1a, L1b, and L2 if B-type or similar fabric exists in the cold forearc mantle wedge. However, Abers et al. (2017) show that the cold forearc part of the mantle wedge in this region is relatively dry and thus is unlikely to support B-type fabric. Furthermore, Mehl et al. (2003) identify fabrics from exhumed mantle rocks found in the nearby relic Talkeetna arc and advocate that they are a product of arc-parallel flow in the mantle wedge. Kneller et al. (2007) show that along strike variations in slab dip and/or oblique subduction can produce different flow directions at different depths. Our region displays a change in slab dip along strike, oblique subduction, and a similar splitting pattern to the two examples in Kneller et al. (2007). This suggests that a model closer aligned with Kneller et al. (2007) is more likely than 2D corner flow with B-type fabric in the cold mantle wedge forearc.

Our interpretation of local splitting results is depicted in Figure 4b. The two-headed red arrow in the Pacific plate represents anisotropic structure in the subducting lithosphere. The overlying red bars represent local splitting observations that correspond to the two-headed red arrow and thus anisotropy in the slab lithosphere. The backarc shows 2D corner flow (orange curved arrow) with a change in mineral, structure, or flow in the cold forearc mantle (blue triangle), and the overlying orange and blue bars are the observed splitting patterns that correspond to anisotropy in their underlying and same colored regions. The depicted transition from arc-perpendicular splitting in the backarc (orange) to arc-parallel in the forearc (blue) due to a change in flow direction has been previously predicted (Kneller et al., 2007) and is supported by the local splitting observations and subduction geometry of this study.

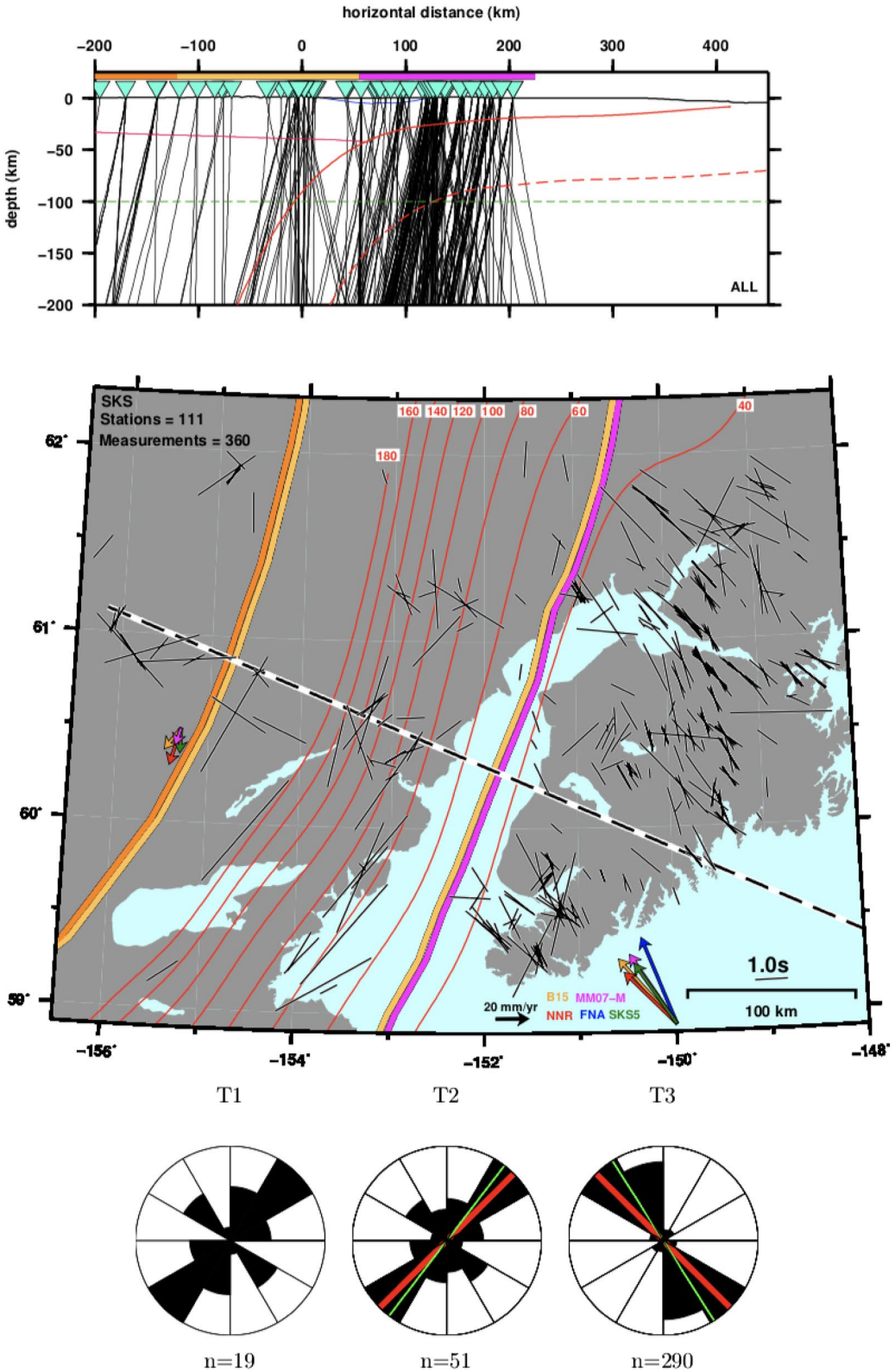

Figure 7. SKS measurements in this study. All 360 high-quality measurements are shown. (top) Cross section showing ray paths. The green dashed line at 100 km depth shows where the splitting measurement is projected to in the map below. (middle) SKS splitting measurements, each plotted with its orientation parallel to ϕ and length scaled to δt. Black and white dashed line represents the cross section seen above. Plate motion vectors are described in Figure S5. The interpreted splitting regions from west to east, are: T1 (orange), T2 (yellow), and T3 (magenta); (bottom) Rose diagrams for the splitting regions.

	outer mantle wedge	inner mantle wedge	mantle cold wedge	forearc
depth to slab	(no slab)	80–160 km	50–80 km	<40 km
mantle thickness	(all mantle)	40–120 km	10–40 km	(none)
local region	L1b	L1a	L2	L3
	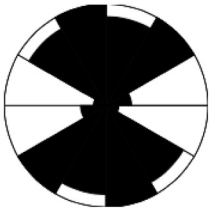	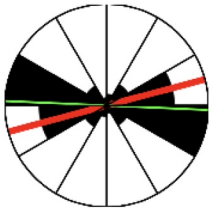		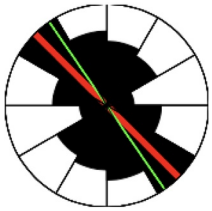
	n=33	n=275	n=258	n=112
SKS region	T1	T2		T3
	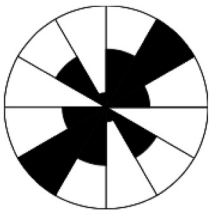	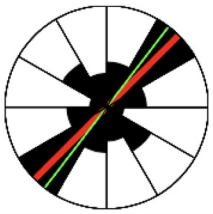		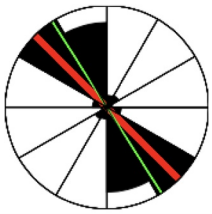
	n=19	n=51		n=290

Figure 8. Comparison of local splitting (top row: from Figure S5) and SKS splitting (bottom row: from Figure 7) results, plotted as rose diagrams of measured fast directions. The number below each rose diagram indicates the number of measurements; the total number of measurements is 678 (local S from non-crustal events) and 360 (SKS). The SKS region T2 spans local regions L1a and L2, but most of its measurements cover the area corresponding with L1a.

4.1. Forward Modeling

Forward modeling involves specifying an anisotropic model and a set of ray paths and then calculating the expected fast direction of splitting and delay time for each raypath. We performed forward modeling for a preliminary set of anisotropic structures to provide a stronger foundation for interpreting subsurface structures from the splitting results in our regions. Anisotropic model parameters include: thickness and orientation of layer, anisotropic mineral type, orientation of anisotropic fabric within layer, and strength of anisotropy. The fabrics were generated in MSAT (Walker & Wookey, 2012) by taking the elasticity tensor of olivine (for most models), mixing 20% of the full anisotropic tensor with 80% of its isotropic average (equivalent to 20% alignment of crystals), and then rotating the fast direction as appropriate. This is done in one or two layers. We assumed the dominant anisotropic signal is in the mantle and thus used incidence angle at the mantle midpoint of the raypath in the forward modeling calculations.

Our forward modeling of various mantle fabrics showed that no simple one-layer or two-layer model fit all of the data well. Some of the fabrics tested include: horizontal fabric aligned in the direction of plate motion (azimuth − 20°), dipping 45° down the dip of the slab (azimuth 300°), foliation parallel to the slab surface, an along-strike fast fabric, and two layer tests by combinations of some of the listed fabrics. These models represent realistic physical settings. For example, the foliation parallel to slab surface model is generated using

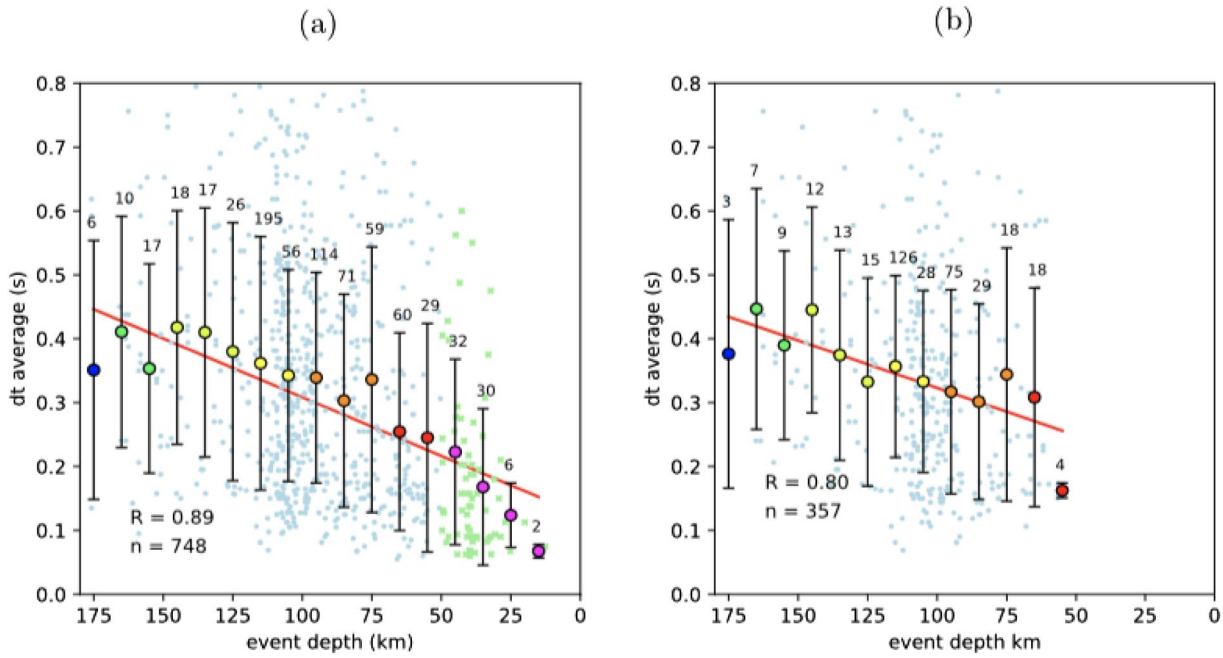

Figure 9. Average local splitting time versus event depth. The correlation between depth and δt suggests that the mantle wedge is anisotropic. (a) Each large filled in circle is the average δt of all measurements from events having depths ±5 km from the target depth. The error bar shows the standard deviation. Each individual measurement is plotted as a blue dot (depth ≥50 km; 678 measurements) or green x (depth < 50 km; 70 measurements). (b) Same as (a) but for the subset of 357 measurements sampling the mantle wedge (e.g., Figure 5).

a serpentine (antigorite) anisotropy tensor with partial foliation. The along-strike fast fabric is represented by olivine fast axes aligned horizontally along strike, as postulated by either along-strike flow from SKS or B-type fabric (azimuth 30°). Figure 10 shows a comparison of modeled and observed splitting parameters for stations that sample the hot part of the mantle wedge (N19K) and the colder forearc mantle wedge (N20 K). The splitting patterns shown by these stations exhibit the previously discussed sharp transition from region L1a to region L2. The fabric here represents 2D corner flow, fits N19K well, but not N20K. This demonstrates that a simple fabric cannot fit all the observations, and that the modeling may need to consider a change in fabric across this region.

Splitting measurements are strongly dependent on incidence angle and some of the lateral variation in the observed splitting patterns could be due to changes in incidence angle rather than fabric. Our forward modeling does take incidence angle into account and can not produce good fits for all parts of the mantle wedge from our simple models. This indicates that further modeling is needed, including lateral variations in the chosen model fabrics, to produce the sharp changes in splitting patterns shown across the previously defined regions. Rather than engage in increasingly complex ad hoc modeling with large numbers of free parameters, we stop after the simple tests done here and defer more realistic, geodynamically plausible models to future studies.

5. Conclusion

We have analyzed shear-wave splitting in the Cook Inlet region of the Alaska subduction zone for local S waves from intraslab earthquakes and for teleseismic SKS waves. Recording of intraslab earthquakes from SALMON stations (2015–2017) and nearby stations provides enhanced sampling of the mantle wedge, relative to coverage from SKS data. Our analyses provide new constraints on mantle flow and anisotropic structures in the Cook Inlet region.

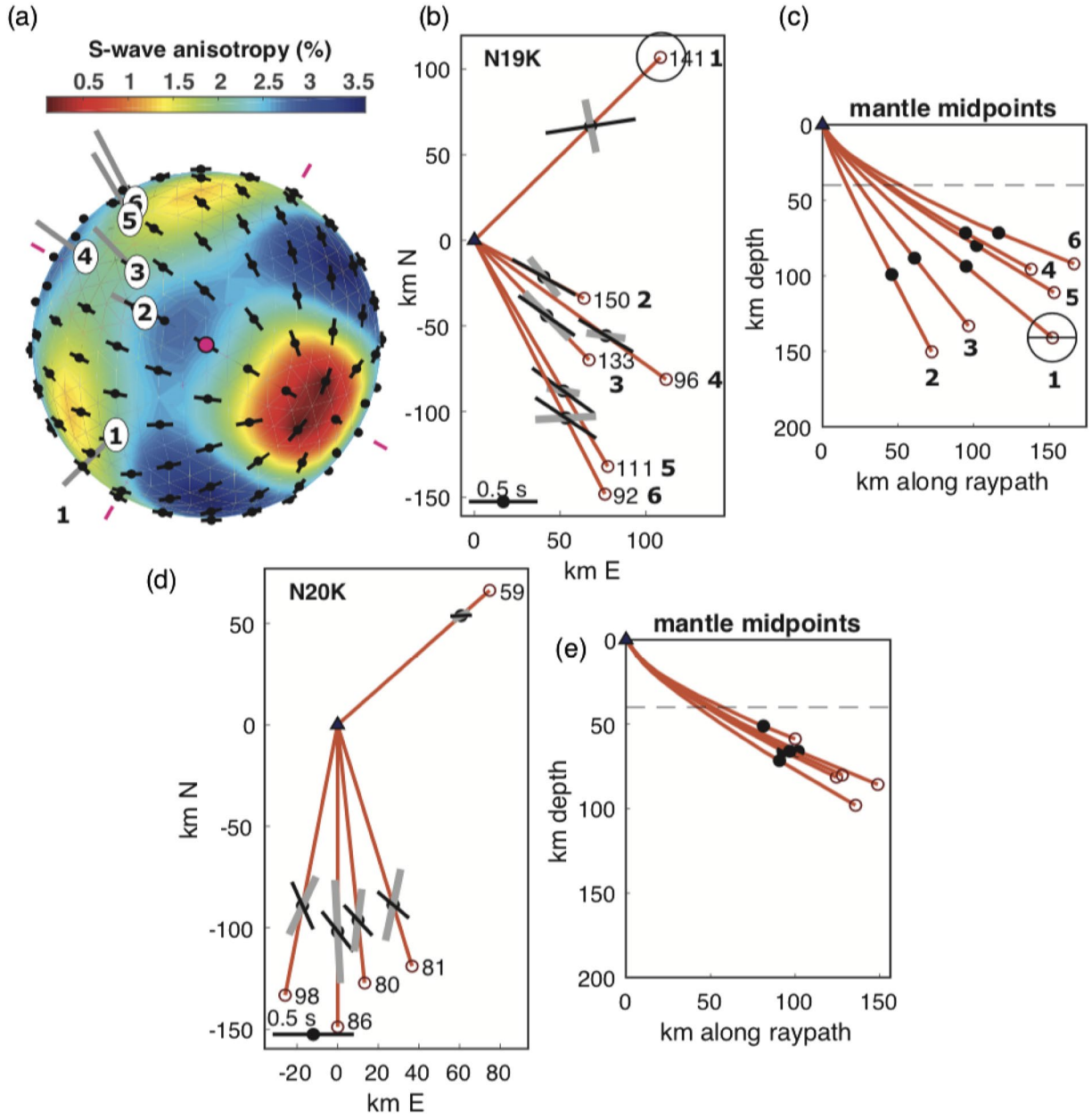

Figure 10. Predicted splitting for an anisotropic fabric with a 45° dip and 300° dip direction, which approximates the orientation of the subducting slab. (a) Upper-hemisphere stereonet showing strength of anisotropy and splitting directions. Gray lines point to exit points of rays from six earthquakes to N19 K and sampling the mantle wedge. The bold numbers 1–6 are labeled in (b and c) as well. (b) Map-view splitting along ray paths, predicted (black bar) and observed (gray bar). The text number is depth in km. (c) Ray paths in cylindrical projection showing depth versus distance from station. In (b) and (c), open circles denote earthquakes labeled by depth in (b); triangle denotes the seismometer; dashed line in (c) shows nominal 40 km upper-plate Moho; filled circles show ray mantle midpoint half way from earthquake to Moho. (d) and (e): same as (b and c) but for station N20K. Five different events are considered. Models generated by MSAT (Walker & Wookey, 2012).

The following conclusions can be made about anisotropy in the Alaska subduction zone.

1. The correlation between depth of local event and δt for stations overlying ≥50 km of wedge indicates that the mantle wedge is anisotropic.
2. The dominantly arc-perpendicular and plate convergence fast directions for local measurements that sample the wedge suggest 2D corner flow in the arc/backarc (Figure 4b).

3. The sharp transition to arc-parallel fast directions for local events sampling the cold forearc wedge indicates a change in mineral, structure, or flow when compared to the rest of the mantle wedge.
4. The arc-parallel forearc and arc-perpendicular backarc local splitting patterns corroborate the observations of Wiemer et al. (1999) and Karlowska et al. (2021) and provide improved data coverage for this region.
5. The large splitting delay times for local ray paths that mainly sample slab indicate that the subducting Pacific lithosphere contains significant anisotropy.
6. Both local S and SKS datasets show plate convergence fast directions at the Kenai Peninsula where there is no underlying mantle wedge.

The differences in local S and SKS splitting patterns (Figure 8) and interpreted mantle dynamics shed light on the importance of combining local and teleseismic datasets when studying subduction zone anisotropy. It also emphasizes the need for a better understanding of the frequency dependence of splitting measurements and sensitivities of each phase. Finally, the inability of the simple forward model fabrics to fit all the observed splitting patterns suggests that the anisotropy variations are not due to variable ray angles, but require distinct differences in the anisotropy regime below the arc, forearc, and subducting plate.

Data Availability Statement

All waveforms used in this study are publically avaialable at IRIS. All splitting measurement data can be found in Richards (2020b). Further analysis and figures from this study, beyond the supplementary material, can be found in Richards (2020a).

Acknowledgments
We acknowledge helpful reviews from Jun Nakajima and an anonymous reviewer. C. Tape thanks Doug Christensen and Melissa Moore for leading the SALMON seismic deployment. This work was supported by NSF Grants EAR-1251971 (Tape), EAR-1829447 (Tape), and EAR-1829440 (Abers).

References

Abers, G. A., van Keken, P. E., & Hacker, B. R. (2017). The cold and relatively dry nature of mantle forearcs in subduction zones. *Nature Geoscience*, *10*, 333–337. https://doi.org/10.1038/NGEO2922

Abt, D. L., Fischer, K. M., Abers, G. A., Strauch, W., Protti, J. M., & González, V. (2009). Shear wave anisotropy beneath Nicaragua and Costa Rica: Implications for flow in the mantle wedge. *Geochemistry, Geophysics, Geosystems*, *10*(5). https://doi.org/10.1029/2009GC002375

Argus, D. F., Gordon, R. G., & DeMets, C. (2011). Geologically current motion of 56 plates relative to the no-net-rotation reference frame. *Geochemistry, Geophysics, Geosystems*, *12*. https://doi.org/10.1029/2011GC003751

Becker, T. W., Schaeffer, A. J., Lebedev, S., & Conrad, C. P. (2015). Toward a generalized plate motion reference frame. *Geophysical Research Letters*, *42*, 3188–3196. https://doi.org/10.1002/2015GL063695

Christensen, D. H., & Abers, G. A. (2010). Seismic anisotropy under central Alaska from SKS splitting observations. *Journal of Geophysical Research*, *115*. https://doi.org/10.1029/2009JB006712

Christensen, D. H., Abers, G. A., & McKnight, T. L. (2003). Mantle anisotropy beneath the Alaska range inferred from *S*-wave splitting observations: Results from BEAAR. *Eos Transactions American Geophysical Union*, *84*(46) Abstract No. S31C-0782.

Crotwell, H. P., Owens, T. J., & Ritsema, J. (1999). The TauP Toolkit: Flexible Seismic travel-time and ray-path utilities. *Seismological Research Letters*, *70*(2), 154–160. https://doi.org/10.1785/gssrl.70.2.154

Davies, J., Sykes, L., House, L., & Jacob, K. (1981). Shumagin seismic gap, Alaska Peninsula: History of great earthquakes, tectonic setting, and evidence for high seismic potential. *Journal of Geophysical Research*, *86*(B5), 3821–3855. https://doi.org/10.1029/jb086ib05p03821

Doubrovine, P. V., Steinberger, B., & Torsvik, T. H. (2012). Absolute plate motions in a reference frame defined by moving hot spots in the Pacific, Atlantic, and Indian oceans. *Journal of Geophysical Research*, *117*, 1–30. https://doi.org/10.1029/2011JB009072

Eberhart-Phillips, D., Christensen, D. H., Brocher, T. M., Hansen, R., Ruppert, N. A., Haeussler, P. J., & Abers, G. A. (2006). Imaging the transition from Aleutian subduction to Yakutat collision in central Alaska, with local earthquakes and active source data. *Journal of Geophysical Research*, *111*. https://doi.org/10.1029/2005JB004240

Favier, N., & Chevrot, S. (2003). Sensitivity kernels for shear wave splitting in transverse isotropic media. *Geophysical Journal International*, *153*, 213–228. https://doi.org/10.1046/j.1365-246X.2003.01894.x

Ferris, A., Abers, G. A., Christensen, D. H., & Veenstra, E. (2003). High resolution image of the subducted Pacific (?) plate beneath central Alaska, 50-150 km depth. *Earth and Planetary Science Letters*, *214*, 575–588. https://doi.org/10.1016/s0012-821x(03)00403-5

Fisher, M. A., & Magoon, L. B. (1978). Geologic framework of lower cook inlet. *American Association of Petroleum Geologists*, *62*(3), 373–402.

Freymueller, J. T., Woodard, H., Cohen, S. C., Cross, R., Elliott, J., Larsen, C. F., et al. (2008). Active deformation processes in Alaska, based on 15 years of GPS measurements. In J. T. Freymueller, P. J. Haeussler, R. Wesson, & G. Ekström (Eds.), Active tectonics and seismic potential of Alaska (Vol. 179, pp. 1–42). American Geophysical Union.

Fu, Y., & Freymueller, J. T. (2013). Repeated large slow slip events at the southcentral Alaska subduction zone. *Earth and Planetary Science Letters*, *375*, 303–311. https://doi.org/10.1016/j.epsl.2013.05.049

Hacker, B. R., & Abers, G. A. (2012). Subduction Factory 5: Unusually low Poisson's ratios in subduction zones from elastic anisotropy of peridotite. *Journal of Geophysical Research*, *117*. https://doi.org/10.1029/2012JB009187

Hall, C. E., Fischer, K. M., Parmentier, E. M., & Blackman, D. K. (2000). The influence of plate motions on three-dimensional back arc mantle flow and shear wave splitting. *Journal of Geophysical Research*, *105*, 28009–28033. https://doi.org/10.1029/2000JB900297

Hammond, J. O. S., Wookey, J., Kaneshima, S., Inoue, H., Yamashina, T., & Harjadi, P. (2010). Systematic variation in anisotropy beneath the mantle wedge in the Java-Sumatra subduction system from shear-wave splitting. *Physics of the Earth and Planetary Interiors*, *178*, 189–201. https://doi.org/10.1016/j.pepi.2009.10.003

Hanna, J., & Long, M. D. (2012). SKS splitting beneath Alaska: Regional variability and implications for subduction processes at a slab edge. *Tectonophysics*, *530–531*, 272–285. https://doi.org/10.1016/j.tecto.2012.01.003

Hayes, G. P., Moore, G. L., Portner, D. E., Hearne, M., Flamme, H., Furtney, M., & Smoczyk, G. M. (2018). Slab2, a comprehensive subduction zone geometry model. *Science*, *362*, 58–61. https://doi.org/10.1126/science.aat4723

Holtzman, B. K., & Kendall, J.-M. (2010). Organized melt, seismic anisotropy, and plate boundary lubrication. *Geochemistry, Geophysics, Geosystems*, *11*(12). https://doi.org/10.1029/2010gc003296

Horn, C., Bouilhol, P., & Skemer, P. (2020). Serpentinization, deformation, and seismic anisotropy in the subduction Mantle Wedge. *Geochemistry, Geophysics, Geosystems*, *21*(4), e2020GC008950. https://doi.org/10.1029/2020GC008950

Jadamec, M. A., & Billen, M. I. (2010). Reconciling surface plate motions with rapid three-dimensional mantle flow around a slab edge. *Nature*, *465*, 338–341. https://doi.org/10.1038/nature09053

Jadamec, M. A., & Billen, M. I. (2012). The role of rheology and slab shape on rapid mantle flow: Three-dimensional numerical models of the Alaska slab edge. *Journal of Geophysical Research*, *117*. https://doi.org/10.1029/2011JB008563

Jarrard, R. D. (1986). Relations among subduction parameters. *Reviews of Geophysics*, *24*(2), 217–284. https://doi.org/10.1029/rg024i002p00217

Jung, H., & Karato, S. (2001). Water-induced fabric transitions in olivine. *Science*, *293*, 1460–1463. https://doi.org/10.1126/science.1062235

Karato, S.-i., Jung, H., Katayama, I., & Skemer, P. (2008). Geodynamic significance of seismic anisotropy of the upper mantle: New insights from laboratory studies. *Annual Review of Earth and Planetary Sciences*, *36*, 59–95. https://doi.org/10.1146/annurev.earth.36.031207.124120

Karlowska, E., Bastow, I. D., Rondenay, S., Martin-Short, R., & Allen, R. M. (2021). The development of seismic anisotropy below south-central Alaska: Evidence from local earthquake shear wave splitting. *Geophysical Journal International*, *225*, 548–554. https://doi.org/10.1093/gji/ggaa603

Kneller, E. A., van Keken, P. E., Karato, S.-i., & Park, J. (2005). B-type olivine fabric in the mantle wedge: Insights from high-resolution non-Newtonian subduction zone models. *Earth and Planetary Science Letters*, *237*, 781–797. https://doi.org/10.1016/j.epsl.2005.06.049

Kneller, E. A., van Keken, P. E., Katayama, I., & Karato, S. (2007). Stress, strain, and B-type olivine fabric in the fore-arc mantle: Sensitivity tests using high-resolution steady-state subduction zone models. *Journal of Geophysical Research*, *112*, 1–17. https://doi.org/10.1029/2006JB004544

Koehler, R. D., Farrell, R.-E., Burns, P. A. C., & Combellick, R. A. (2012). *Quaternary faults and folds in Alaska: A digital database*. (Alaska Division of Geological & Geophysical Surveys 141, p. 31. 1 sheet, scale 1:3,700,000). https://doi.org/10.14509/23944

León Soto, G., & Valenzuela, R. W. (2013). Corner flow in the Isthmus of Tehuantepec, Mexico inferred from anisotropy measurements using local intraslab earthquakes. *Geophysical Journal International*, *195*(2), 1230–1238. https://doi.org/10.1093/gji/ggt291

Li, S., Freymueller, J., & McCaffrey, R. (2016). Slow slip events and time-dependent variations in locking beneath Lower Cook Inlet of the Alaska-Aleutian subduction zone. *Journal of Geophysical Research: Solid Earth*, *121*, 1060–1079. https://doi.org/10.1002/2015JB012491

Long, M. D., & Becker, T. W. (2010). Mantle dynamics and seismic anisotropy. *Earth and Planetary Science Letters*, *297*, 341–354. https://doi.org/10.1016/j.epsl.2010.06.036

Long, M. D., & Silver, P. G. (2008). The subduction zone flow field from seismic anisotropy: A global view. *Science*, *319*, 315–318. https://doi.org/10.1126/science.1150809

Long, M. D., & van der Hilst, R. D. (2006). Shear wave splitting from local events beneath the Ryukyu arc: Trench-parallel anisotropy in the mantle wedge. *Physics of the Earth and Planetary Interiors*, *155*, 300–312. https://doi.org/10.1016/j.pepi.2006.01.003

Long, M. D., & Wirth, E. A. (2013). Mantle flow in subduction systems: The mantle wedge flow field and implications for wedge processes. *Journal of Geophysical Research: Solid Earth*, *118*, 583–606. https://doi.org/10.1002/jgrb.50063

Marson-Pidgeon, K., & Savage, M. K. (1997). Frequency-dependent anisotropy in Wellington, New Zealand. *Geophysical Research Letters*, *24*(24), 3297–3300. https://doi.org/10.1029/97gl03274

Maus, S., Barckhausen, U., Berkenbosch, H., Bournas, N., Brozena, J., Childers, V., et al. (2009). EMAG2: A 2-arc min resolution Earth magnetic anomaly grid compiled from satellite, airborne, and marine magnetic measurements. *Geochemistry, Geophysics, Geosystems*, *10*(8). https://doi.org/10.1029/2009GC002471

McPherson, A. M., Christensen, D. H., Abers, G. A., & Tape, C. (2020). Shear wave splitting and mantle flow beneath Alaska. *Journal of Geophysical Research: Solid Earth*, *125*, 1–18. https://doi.org/10.1029/2019JB018329

Mehl, L., Hacker, B. R., Hirth, G., & Kelemen, P. B. (2003). Arc-parallel flow within the mantle wedge: Evidence from the accreted Talkeetna arc, south central Alaska. *Journal of Geophysical Research*, *108*(B8). https://doi.org/10.1029/2002JB002233

Miller, M. S., & Moresi, L. (2018). Mapping the Alaskan Moho. *Seismological Research Letters*, *89*(6), 2430–2436. https://doi.org/10.1785/0220180222

Morgan, W. J., & Morgan, J. P. (2007). Plate velocities in the hotspot reference frame. In G. R. Foulger, & D. M. Jurdy (Eds.), *Plates, plumes, and planetary processes* (pp. 65–78). Geological Society of America.

Nakajima, J., & Hasegawa, A. (2004). Shear-wave polarization anisotropy and subduction-induced flow in the mantle wedge of northeastern Japan. *Earth and Planetary Science Letters*, *225*, 365–377. https://doi.org/10.1016/j.epsl.2004.06.011

Naugler, F. P., & Wageman, J. M. (1973). Gulf of Alaska: Magnetic anomalies, fracture zones, and plate interaction. *Geological Society of America Bulletin*, *84*(5), 1575–1584. https://doi.org/10.1130/0016-7606(1973)84<1575:goamaf>2.0.co;2

Nuttli, O. (1961). The effect of the earth's surface on the *S* wave particle motion. *Bulletin of the Seismological Society of America*, *51*(2), 237–246.

Ohta, Y., Freymueller, J., Hreinsdóttir, S., & Suito, H. (2006). A large slow slip event and the depth of the seismogenic zone in the south central Alaska subduction zone. *Earth and Planetary Science Letters*, *247*, 108–116. https://doi.org/10.1016/j.epsl.2006.05.013

Perttu, A., Christensen, D., Abers, G., & Song, X. (2014). Insights into mantle structure and flow beneath Alaska based on a decade of observations of shear wave splitting. *Journal of Geophysics Research: Solid Earth*, *119*, 8366–8377. https://doi.org/10.1002/2014JB011359

Richards, C. (2020a). *Anisotropy in the Alaska Subduction Zone: Shear-wave splitting observations from local and teleseismic earthquakes* (Master's thesis). University of Alaska Fairbanks.

Richards, C. (2020b). *Shear-wave splitting observations from local and teleseismic earthquakes recorded in Alaska*. Retrieved from http://hdl.handle.net/11122/11004

Rondenay, S., Montési, L. G. J., & Abers, G. A. (2010). New geophysical insight into the origin of the Denali volcanic gap. *Geophysical Journal International*, *182*, 613–630. https://doi.org/10.1111/j.1365-246x.2010.04659.x

Ross, Z. E., White, M. C., Vernon, F. L., & Ben-Zion, Y. (2016). An improved algorithm for Real-TimeS-Wave picking with application to the (Augmented) ANZA network in Southern California. *Bulletin of the Seismological Society of America*, *106*(5), 2013–2022. https://doi.org/10.1785/0120150230

Savage, M. K. (1999). Seismic anisotropy and mantle deformation: What have we learned from shear wave splitting?. *Reviews of Geophysics*, *37*(1), 65–106. https://doi.org/10.1029/98rg02075

Savage, M. K., Wessel, A., Teanby, N. A., & Hurst, A. W. (2010). Automatic measurement of shear wave splitting and applications to time varying anisotropy at Mount Ruapehu volcano, New Zealand. *Journal of Geophysical Research*, *115*. https://doi.org/10.1029/2010JB007722

Schlaphorst, D., Kendall, J.-M., Baptie, B., Latchman, J. L., & Tait, S. (2017). Gaps, tears and seismic anisotropy around the subducting slabs of the antilles. *Tectonophysics*, *698*, 65. https://doi.org/10.1016/j.tecto.2017.01.002

Silver, P. G., & Chan, W. W. (1991). Shear wave splitting and subcontinental mantle deformation. *Journal of Geophysical Research*, *96*(B10), 16429–16454. https://doi.org/10.1029/91jb00899

Silver, P. G., & Savage, M. K. (1994). The interpretation of shear-wave splitting parameters in the presence of two anisotropic layers. *Geophysical Journal International*, *119*, 949–963. https://doi.org/10.1111/j.1365-246x.1994.tb04027.x

Song, T.-R. A., & Kawakatsu, H. (2013). Subduction of oceanic asthenosphere: A critical appraisal in central Alaska. *Earth and Planetary Science Letters*, *367*, 82–94. https://doi.org/10.1016/j.epsl.2013.02.010

Spetzler, J., & Snieder, R. (2004). The Fresnel volume and transmitted waves. *Geophysics*, *69*(3), 653–663. https://doi.org/10.1190/1.1759451

Tape, C., Christensen, D., Moore-Driskell, M. M., Sweet, J., & Smith, K. (2017). Southern Alaska Lithosphere and Mantle Observation Network (SALMON): A seismic experiment covering the active arc by road, boat, plane, and helicopter. *Seismological Research Letters*, *88*(4), 1185–1202. https://doi.org/10.1785/0220160229

Teanby, N. A., Kendall, J.-M., & van der Baan, M. (2004). Automation of shear-wave splitting measurements using cluster analysis. *Bulletin of the Seismological Society of America*, *94*(2), 453–463. https://doi.org/10.1785/0120030123

Uchida, N., Nakajima, J., Wang, K., Takagi, R., Yoshida, K., Nakayama, T., et al. (2020). Stagnant forearc mantle wedge inferred from mapping of shear-wave anisotropy using S-net seafloor seismometers. *Nature Communications*, *11*, 1–8. https://doi.org/10.1038/s41467-020-19541-y

van Keken, P. E. (2003). The structure and dynamics of the mantle wedge. *Earth and Planetary Science Letters*, *215*(3), 323–338. https://doi.org/10.1016/s0012-821x(03)00460-6

Venereau, C. M. A., Martin-Short, R., Bastow, I. D., Allen, R. M., & Kounoudis, R. (2019). The role of variable slab dip in driving mantle flow at the eastern edge of the Alaskan subduction margin: Insights from shear-wave splitting. *Geochemistry, Geophysics, Geosystems*, *20*, 2433–2448. https://doi.org/10.1029/2018GC008170

Walker, A. M., & Wookey, J. (2012). MSAT-A new toolkit for the analysis of elastic and seismic anisotropy. *Computers & Geosciences*, *49*, 81–90. https://doi.org/10.1016/j.cageo.2012.05.031

Wech, A. G. (2016). Extending Alaska's plate boundary: Tectonic tremor generated by Yakutat subduction. *Geology*, *44*(7), 587–590. https://doi.org/10.1130/G37817.1

Wei, M., McGuire, J. J., & Richardson, E. (2012). A slow slip event in the south central Alaska Subduction Zone and related seismicity anomaly. *Geophysical Research Letters*, *39*. https://doi.org/10.1029/2012GL052351

Wessel, A. (2000). *Automatic shear wave splitting measurements at Mt. Ruapehu Volcano, New Zealand* (M.S. thesis). Victoria University of Wellington.

Wiemer, S., Tytgat, G., Wyss, M., & Duenkel, U. (1999). Evidence for shear-wave anisotropy in the mantle wedge beneath south central Alaska. *Bulletin of the Seismological Society of America*, *89*(5), 1313–1322.

Wirth, E., & Long, M. D. (2010). Frequency-dependent shear wave splitting beneath the Japan and Izu-Bonin subduction zones. *Physics of the Earth and Planetary Interiors*, *181*, 141–154. https://doi.org/10.1016/j.pepi.2010.05.006

Yang, X., Fischer, K. M., & Abers, G. A. (1995). Seismic anisotropy beneath the Shumagin Islands segment of the Aleutian-Alaska subduction zone. *Journal of Geophysical Research*, *100*(B9), 18165–18177. https://doi.org/10.1029/95jb01425